1.34 Determination of local volumetric rate of photon absorption of $NiFe_2O_4$ photocatalyst in aqueous suspensions under visible light

Jorge Domínguez-Arvizu, Alejandro López Ortiz, J. M. Salinas-Gutierrez, M. J. Meléndez-Zaragoza, Virginia Collins-Martínez

[1]Centro de Investigación en Materiales Avanzados S. C., Miguel de Cervantes 120, CP. 31136, Chihuahua, México

* Corresponding author: virginia.collins@cimav.edu.mx, jorge.dominguez@cimav.edu.mx

ABSTRACT

In the present work the absorption (κ) and scattering (σ) coefficients were determined for $NiFe_2O_4$ nanoparticles in aqueous suspensions. The photocatalyst was previously synthetized by a modified Pechini method, measurements were carried out through UV/Visible spectroscopy, and experimental data were fitted with a new proposed model called 3-dim-3-dir. The resultant coefficients were used to solve the radiative transfer equation (RTE) using a discrete ordinated method (DOM) in order to determine the local volumetric rate of photon absorption (LVRPA) in a proposed reactor design model employing $NiFe_2O_4$ as photocatalyst.

Keywords: Visible light photocatalyst; LVRPA; Radiative transfer equation; absorption and scattering coefficients

1. Introduction

Nowadays, fossil fuels supply about 90% of energy in transportation and industrial sectors. In 2013 energy consumption reached approximately 17 TW and according to the U.S. EIA (Energy information administration) a 56% increment is expected for 2040 where the fossil fuels will comprise the 78%. Massive utilization of fossil fuels has been responsible for climate change due to greenhouse gases generation and pollutant emissions, besides to produce other harmful effects such as acid rain, increasing ozone concentration in urban zones and particle emissions affecting the environment. For those reasons, global interests have been oriented towards developing new energy systems capable of balancing energy supplies and current demands, protecting the environment, and ensuring reliable energy power sources as well as economic viability [1-4].

Within proposed alternatives, hydrogen as energy carrier is considered advantageous with respect to fossil fuels as numerous studies suggest hydrogen would be a more economic and cleaner energy source. Furthermore, this fuel has 2.75 times higher energy yield (122 kJ/g) than typical fossil fuels. To be economically sustainable hydrogen must be obtained from a renewable source e.g. solar energy. While, photocatalysis is one of the most promising technologies for this purpose, since H_2 and O_2 molecules can be directly obtained from a water splitting process through light irradiation of semiconductor materials. Among main features of these photocatalyst must present: a high efficiency and photocorrosion stability, not be harmful to the environment and to be active under visible light [5, 6].

At this moment, TiO_2 is the most common and widely studied photocatalyst, this is due to its high stability and photocorrosion resistance. There is a considerable number of publications where reactor modeling and design have been carried out for hydrogen production [7, 8] and water/air purification [9, 10] with this material. Nevertheless, TiO_2 efficiency is very low under visible light, since this process is limited to UV light sources, which unfortunately comprises 4% of solar light irradiation. It is in this sense, that the search of a highly efficient active material under visible light (which comprises the 43% of the solar energy) has become one of the most important challenges in today's photoreactor design [11, 12].

As an alternative, transition metals ferrites have in general a low cost, high photocorrosion resistance and activity under visible light. Selection of these materials is based on their redox activity and specifically on their ability to store oxygen in its crystalline lattice. This phenomena are due to the tendency of these materials to form oxygen vacancies when they are synthetized by methods that generate reducing atmospheres while increasing its photocatalytic activity [11].

However, at the present, there are no publications related to photoreactor designs that comprise these materials. Therefore, it is necessary to determine their optical properties in aqueous suspensions, i.e. the absorption coefficient (κ), scattering coefficient (σ) and the phase function p (Ω´→Ω), which only have been determined for TiO_2 at the present using methodologies involving UV/visible spectroscopy and a mathematical model called 1-dim-1dir [13, 14].

These optical properties play an important role in determining the radiation distribution of heterogeneous photoreactors, since those are required to solve the radiative transfer equation (RTE) [15]:

$$\frac{dI_\lambda(s,\Omega)}{ds} = -\kappa_\lambda I_\lambda(s,\Omega) - \sigma_\lambda I_\lambda(s,\Omega) + \frac{1}{4\pi}\sigma_\lambda \int_0^{4\pi} p(\Omega' \rightarrow \Omega)\, I(s,\Omega')d\Omega' \qquad \textbf{(2)}$$

RTE solution will provide the radiation intensity distribution in the reactor, and with this information it is possible to calculate the local volumetric rate of photon absorption (LVRPA), a parameter directly related to the photochemical reaction kinetics [12, 16].

This work is aimed to determine the absorption and scattering coefficients of $NiFe_2O_4$ aqueous suspensions previously synthetized by a modified Pechini's method in order to calculate the LVRPA in a proposed design of an aqueous photoreactor by means of the RTE solution. All of this, aiming to take advantage of $NiFe_2O_4$ as a potential photocatalytic material for hydrogen production under visible light.

2. Materials and Methods

2.1 The phase function

The phase function describes the directional distribution of scattered radiation. In order to choose the appropriate mathematical expression for it, there is a size parameter (ξ) related to the wavelength λ of the radiation inside the reactor and the particle spherical size d_p that needs to be determined through the equation 2.

In order to measure d_p of the particle agglomerates, SEM images were taken in a field emission microscope JEM-2200-FS. Samples were prepared over a carbon coated copper grid by dispersing 1 mg of the material in 1mL of distilled water and sonicating for 20 minutes.

$$\xi = \left[\frac{\pi d_p}{\lambda}\right]_{min} \quad \textbf{(3)}$$

Later, a drop of suspension was applied over the grid and it was exposed to a lamp to evaporate the water. Figure 1 shows an image of $NiFe_2O_4$ nanoparticle agglomerates.

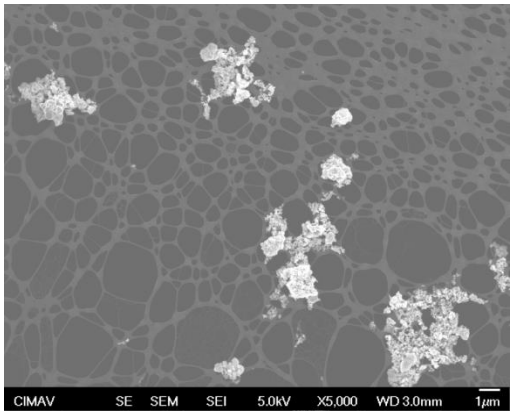

Fig 1. $NiFe_2O_4$ nanoparticles agglomerates formed in aqueous suspensions

An estimate of the size parameter ξ, was obtained by measuring the shortest distance of the agglomerates in various sample zones, where the minimum value of d_p was set to 100 nm, and using the maximum wavelength in the experiments (800 nm), thus obtaining a value equal to 0.4.

According to the assumption that the agglomerates are of spherical shape, the adequate phase function to be used is the following [12]:

$$p(\theta) = 1 + A\cos(\theta) \quad \textbf{(4)}$$

With A= 1, 0, -1 for forward, isotropic and backward scattering, respectively.

2.2 Extinction coefficient

In radiation transport theory, the sum of the scattering and absorption contribution represents the extinction coefficient ($\beta = \sigma + \kappa$). Through absorbance measurements in a heterogeneous medium, the obtained data will provide the "lost" radiation by absorption and light scattering (Figure 2). Thus, the "extinctance" will be obtained through UV/Vis measurements [13].

For the extinction coefficient determination, $NiFe_2O_4$ suspensions were prepared in 100 mL volumetric flasks at 0.13, 0.26, 0.35 y 0.48 g/L with distilled water, which were exposed under sonication during the whole experiment. Quartz cells with 10 mm path length were used and the measurements were carried out in a Perkin Elmer Lambda 35 UV/Vis spectrometer using distilled water as a blank reference.

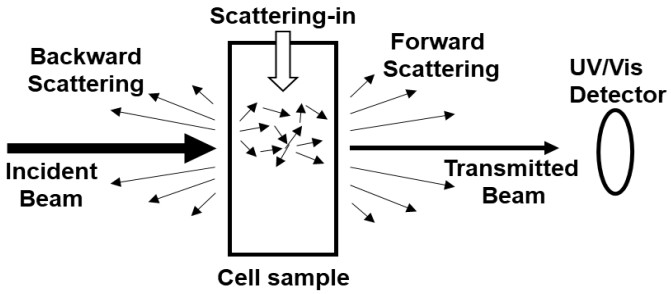

Fig 2. Optical phenomena involved in the determination of the extinction coefficient

With the objective of avoiding an eventual settling of coarser aggregates, readings were punctually carried out from 300 to 800 nm in 100 nm intervals by replacing the suspension every time a measurement was performed.

The extinction coefficient was calculated through the following equation:

$$\beta_\lambda = \frac{2.303 EXT_\lambda}{L} \quad \textbf{(5)}$$

Where *L* is the path length of the quartz cell and EXT_λ denotes the extintance.

Later, a specific extinction coefficient per unit mass was obtained ($\beta^*_\lambda = \beta_\lambda/C_m$) [$m^2/g$] by calculating the slope of the curve through a linear regression of the β_λ vs C_m data that showed a linear relationship.

2.3 Absorption coefficient

By means of transmittance measurements with an integrating sphere model RSA-PE-20 Labsphere, the front scattered and transmitted rays were detected by positioning the quartz cell in front of the sphere. To collect the whole rays mentioned before, a blank with a ~1 reflectance made of Spectralon® material was positioned behind the sphere. The whole system configuration used is shown in Figure 3.

Same conditions as in the extinction coefficient were performed during sample preparation corresponding to 0.10, 0.22, 0.31 and 0.37 g/L concentrations and the absorption coefficient (κ_λ) was obtained through the following equation:

$$\kappa_\lambda = \frac{2.303}{L}\log\frac{1}{T_\lambda} \qquad (6)$$

Where *L* is the path length of the quartz cell and transmittance is T_λ.

A linear regression from C_m vs κ_λ plots (resulting in a linear trend) was carried out in order to obtain a specific absorption coefficient κ^*_λ through the slope of this data. Finally the scattering coefficient σ^*_λ was obtained from the difference $\beta^*_\lambda - \kappa^*_\lambda$.

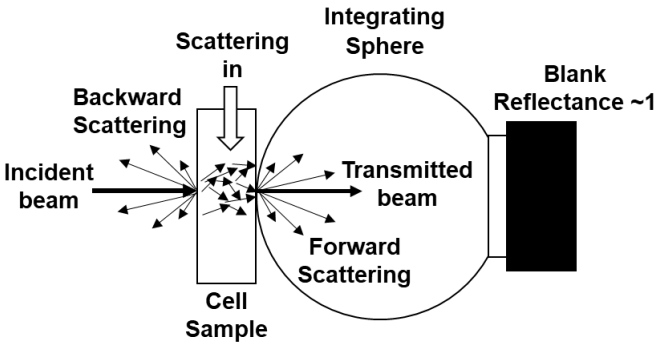

Fig. 3. Scheme configuration to evaluate absorption coefficients in $NiFe_2O_4$ aqueous suspensions

2.4 3-dim-3dir methodology

To adjust the κ^*_λ and σ^*_λ coefficients obtained experimentally, the radiation distribution in the quartz cells was simulated by solving the RTE equation in three dimensions and thee directions with a discrete ordinate method (DOM) in ANSYS FLUENT 17.0.

First, the collimated incident beam was measured in order to introduce its dimensions as a boundary condition (1 mm x 8 mm) with a user defined function (UDF) in ANSYS FLUENT. Only the quartz cell volume that was exposed in the sample cell holder was considered in the model (Figure 4a and 4b), using the refractive index of water of 1.33. The number of volume elements on the mesh was 47424 with 51480 nodes (Figure 4c).

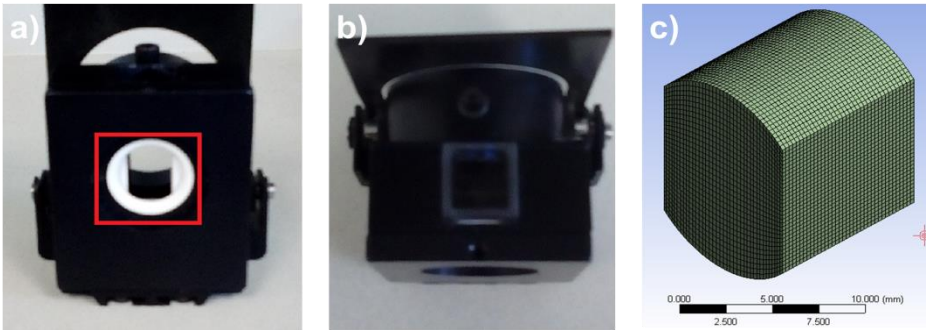

Fig 4. Cell sample zones where physical phenomena was studied, a) and b): two perspectives of the cell sample holder, c): meshing involved in the simulation

The transmittance values were obtained by calculating the ratio between the radiation power in the whole face oriented to the integrating sphere and the collimated beam power using the κ_λ and σ_λ values determined in the transmittance measurements as well as the linear anisotropic phase function with A=1. The values were varied by a trial and error procedure until obtaining the highest coincidence of the experimental with respect to the calculated transmittance. By this procedure, the fitted κ^*_λ and σ^*_λ values were obtained.

2.5 LVRPA determination

2.5.1 Specifications, reactor and lamp dimensions

Reactor dimensions are based on a design reported by Pareek et al. (2004) [16], while lamp specifications were obtained from a GE ARC-SREAM double ended spec sheet: 150 W (1.08×10^{-3} Einsteins/s) power from 300 to 800 nm (Figure 5b). The reactor and lamp dimensions as well as configuration are shown in Figure 5a.

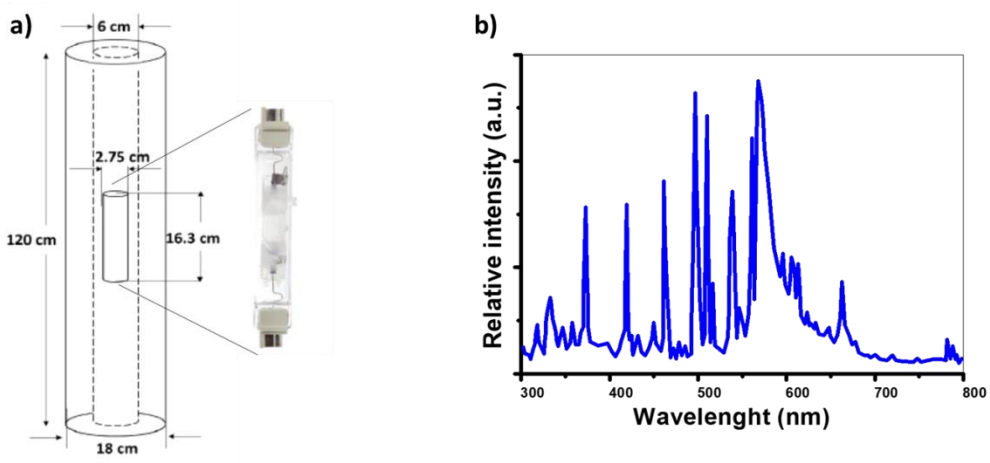

Fig 5. a) Photoreactor system configuration, b) Lamp spectra obtained from 300 to 800 nm

2.5.2 Boundary conditions

In order to compute the radiation intensity at the inner wall of the reactor, the volume source model was used (VSM) [12]:

$$G_v = \frac{K_{v3}}{4\pi} \int_{h=-L}^{h=L} \int_{\eta=0}^{\eta=R} \int_{\phi=-\pi}^{\phi=\pi} \frac{\eta d\phi d\eta dh}{[(rcos\theta - \eta cos\phi)^2 + (rsen\theta - \eta sen\phi)^2 + (z-h)^2]} \quad \textbf{(6)}$$

Where G_v is the radiation intensity at point $Q(r, \theta, z)$ in the reactor wall, L and R the semilenght and lamp radius respectively and K_{v3} the lamp emission power per unit volume.

The VSM equation was introduced as a boundary condition in a semi-transparent wall as a used defined function assuming specular emission. The external walls were considered as an opaque medium with an absorptivity equal to 1 and the meshing consisted of 16040 cylindrical volume elements with 19064 nodes (Figure 8).

Once the radiation distribution on the inner wall was determined, the RTE was solved over the whole reactor space, thus obtaining the radiation intensity value at any point in the reactor, then the LVRPA was calculated by means of the following equation:

$$LVRPA = \langle \kappa^* \rangle I(s, \Omega) \quad \textbf{(7)}$$

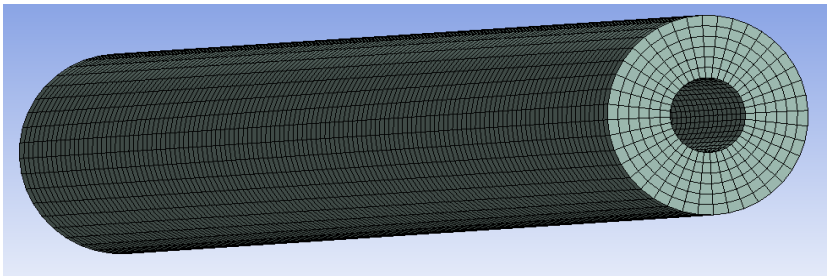

Fig 6. Meshing for the solution of the RTE in the $NiFe_2O_4$ photoreactor

2.5.3 Solver parameters

FLUENT's segregate solver was used to perform the simulations in the photoreactor with a unity relaxation factors for energy and radiation intensity to achieve a faster convergence. To avoid control angle overhanging, a pixilation of 3 x 5 was used. The iterations were performed until residuals were less or equal than 1 x 10^{-6}, a typical convergence history required about 100 – 150 iterations being dependent on the values of σ and κ.

3. Results and Discussion

3.1 Scattering and absorption coefficients

Plots of experimental and fitted specific coefficients are shown in Figure 7. It is possible to observe that obtained values for the extinction coefficient decreased with respect to the experimental ones. This is because possibly not all transmitted radiation was detected in the UV/Vis due to the refractive index of the samples. For example, some of the transmitted beams did not reach the detector. In addition, the corrected values for the absorption coefficient are smaller than the experimental ones too. This is due to the fact that front scattered rays could not be detected by the integrating sphere, thus increasing the "radiation losses" and consequently the computed absorbance in the experiment.

In order to prove the validity of the obtained data, a comparison between experimental and calculated transmittance through the fitted coefficients for 300, 500 and 800 nm (Figure 8) was performed.

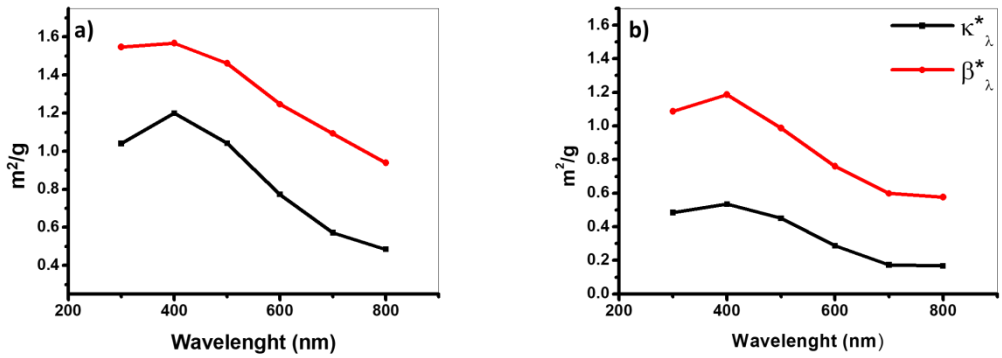

Fig 7. a) Experimental readings of extinction and absorption coefficients, b) Fitted values of extinction and absorption coefficients from 3-dim-3-dir methodology

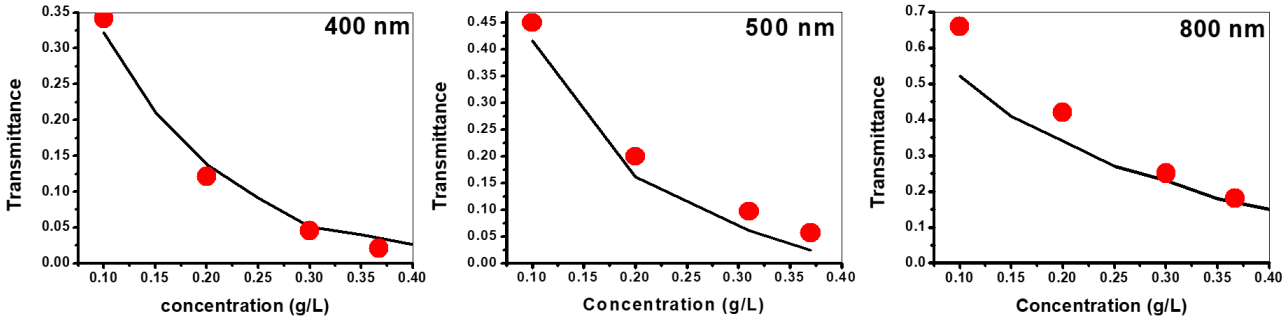

Fig 8. Experimental transmittance values vs calculated at 300, 800 and 500 nm

It can be seen that there exists a good agreement between experimental and the theoretical model despite the refractive index of suspensions was considered the same as water (1.33).

Since calculations of LVRPA in the reactor could be intensive considering the scattering and absorption coefficients wavelength dependence, a wavelength-averaged coefficients were obtained by the following integrations:

$$\langle \kappa^* \rangle = \frac{\int_{300\ nm}^{800\ nm} \kappa_\lambda^* d\lambda}{\langle \lambda \rangle} = 0.35\ m^2/g \quad \textbf{(8)}$$

$$\langle \sigma^* \rangle = \frac{\int_{300\ nm}^{800\ nm} \sigma_\lambda^* d\lambda}{\langle \lambda \rangle} = 0.52\ m^2/g \quad \textbf{(9)}$$

3.2 LVRPA determination

Figure 9 shows results of contour plots for the $NiFe_2O_4$ suspension at 0.1 g/L in radial and three dimensions-axial perspective. As expected, the LVRPA decreases as the radial and axial distance increases. This is because rays during the path between the inner wall and the outer walls are absorbed by the solid photocatalyst, thus suggesting that an optimal distance can be fixed in order to improve the reactor efficiency, which will eventually be translated in a reduction of reactor dimensions. However, kinetic parameters must be obtained in order to obtain more accurate predictions. In order to have a more detailed perspective, LVRPA was calculated and plotted in the two perspectives mentioned before (Figure 10), the range of LVRPA obtained was between $2.22x10^{-4}$ and 1.57 Einstenis/m^3s.

It is important to notice a decrease at 0.1 m in the axial coordinate, having a LVRPA of 0.2 Einstein/m^3s. Therefore, it can be relevant to reduce the reactor length, whereas the decrease of LVRPA in radial distance is not as significant as in the axial coordinate.

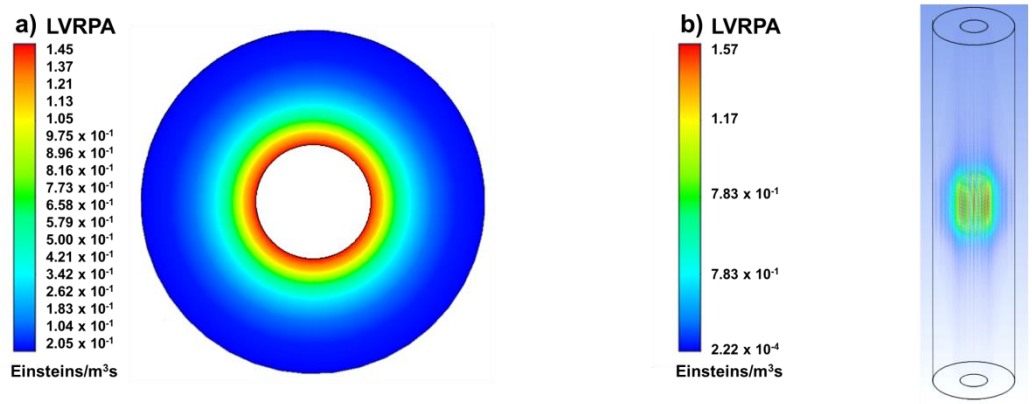

Fig 5. Contours of LVRPA values for the $NiFe_2O_4$ at 0.1 g/L: a) Radial coordinate, b) Axial coordinate

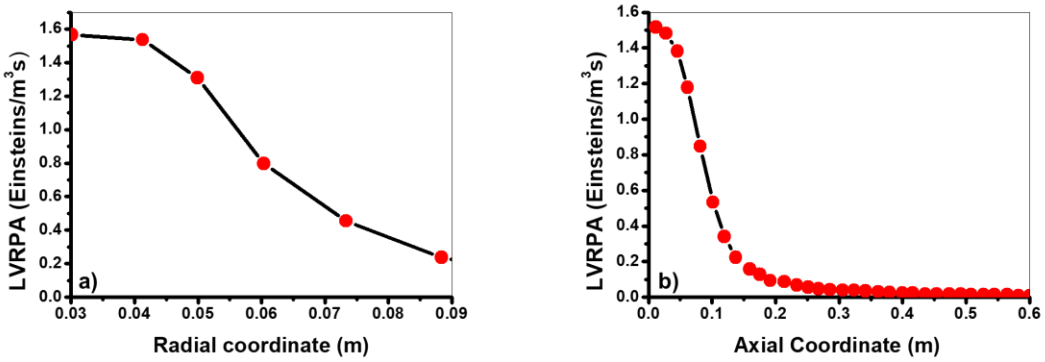

Fig 6. Values of LVRPA at 0.1 g/L at: a) Radial coordinate, b) Axial coordinate

4. Conclusions

A new methodology called 3-dim-3-dir was developed and this showed a good agreement with experimental and theoretical data. Absorption and scattering coefficients of $NiFe_2O_4$ nanoparticles were determined, which values corresponded to 0.354 m^2/g and 0.519 m^2/g respectively. These results can be more accurate if the refractive index of the suspensions is considered. Finally the LVRPA was calculated in the photocatalytic reactor with values between $2.22x10^{-4}$ and 1.57 Einsteins/m^3s.

Aknowledgments

The authors acknowledge M.Sc. Ernesto Guerrero Lestarjette, M. Sc. Karla Campos Venegas, Eng. Wilber Antunez Flores, and Eng. Luis de la Torre Saenz for their contributions to the XRD, SEM, BET, results. Special thanks are given to Laboratorio Nacional de Nanotecnologia in Centro de Investigacion en Materiales Avanzados, S. C., for their support in the use of the facilities.

References

[1] Jafari, T., Moharreri, E., Amin, A. S., Miao, R., Song, W., & Suib, S. L. (2016). Photocatalytic Water Splitting—The Untamed Dream: A Review of Recent Advances. Molecules, 21(7), 900.

[2] Suleman, F., Dincer, I., & Agelin-Chaab, M. (2015). Environmental impact assessment and comparison of some hydrogen production options. International journal of hydrogen energy, 40(21), 6976-6987.

[3] Michaelides, E. E. S. (2012). Alternative energy sources. Springer Science & Business Media.

[4] Won, W., Kwon, H., Han, J. H., & Kim, J. (2017). Design and operation of renewable energy sources based hydrogen supply system: Technology integration and optimization. Renewable Energy, 103, 226-238.

[5] Hosseini, S. E., & Wahid, M. A. (2016). Hydrogen production from renewable and sustainable energy resources: Promising green energy carrier for clean development. Renewable and Sustainable Energy Reviews, 57, 850-866.

[6] Ortiz, A. L., Zaragoza, M. M., & Collins-Martínez, V. (2016). Hydrogen production research in Mexico: A review. International Journal of Hydrogen Energy, 41(48), 23363-23379.

[7] Castedo, A., Uriz, I., Soler, L., Gandía, L. M., & Llorca, J. (2017). Kinetic analysis and CFD simulations of the photocatalytic production of hydrogen in silicone microreactors from water-ethanol mixtures. Applied Catalysis B: Environmental, 203, 210-217.

[8] Salas, S. E. (2013). Photocatalytic Water Splitting Using a Modified $PtTiO_2$. Kinetic Modeling and Hydrogen Production Efficiency (Doctoral dissertation, Ph. D. Thesis, The University of Western Ontario, London, ON, Canada).

[9] Alfano, O.M., Vicente, M., Esplugas, S., Cassano, A.E., 1990. Radiation field inside a tubular multilamp reactor for water and waste water treatment. Ind. Eng. Chem. Res. 29, 1270–1278.

[10] Castrillon, S.R.V., de Lasa, H.I., 2007. Performance evaluation of photocatalytic reactors for air purification using computational fluid dynamics (CFD).Ind. Eng. Chem. Res.46, 5867–5880.

[11] López, Y. O., Vázquez, H. M., Gutiérrez, J. S., Velderrain, V. G., Ortiz, A. L., & Martínez, V. C. (2015). Synthesis method effect of CoFe2O4 on its photocatalytic properties for H 2 production from water and visible light. Journal of Nanomaterials, 16(1), 76.

[12] Boyjoo, Y., Ang, M., & Pareek, V. (2013). Some aspects of photocatalytic reactor modeling using computational fluid dynamics. Chemical Engineering Science, 101, 764-784.

[13] Cabrera, M. I., Alfano, O. M., & Cassano, A. E. (1996). Absorption and scattering coefficients of titanium dioxide particulate suspensions in water. The Journal of Physical Chemistry, 100 (51), 20043-20050.

[14] Satuf, M. L., Brandi, R. J., Cassano, A. E., & Alfano, O. M. (2005). Experimental method to evaluate the optical properties of aqueous titanium dioxide suspensions. Industrial & engineering chemistry research, 44(17), 6643-6649.

[15] Pareek, V., Chong, S., Tadé, M., & Adesina, A. A. (2008). Light intensity distribution in heterogenous photocatalytic reactors. Asia-Pacific Journal of Chemical Engineering, 3(2), 171-201.

[16] Pareek, V. K., & Adesina, A. A. (2004). Light intensity distribution in a photocatalytic reactor using finite volume. AIChE journal, 50(6), 1273-1288.